Eleventh International Conference on CFD in the Minerals and Process Industries
CSIRO, Melbourne, Australia
7-9 December 2015

COMPARISON OF A TWO-FLUID MODEL AND AN EULER-LAGRANGE MODEL FOR SIMULATION OF DENSE GAS-FLUIDIZED BEDS

L. (Lei) YANG, J.T. (Johan) PADDING* and J.A.M. (Hans) KUIPERS

Department of Chemical Engineering and Chemistry, Eindhoven University of Technology, 5600 MB, Eindhoven, The Netherlands
*Corresponding author, E-mail address: J.T.Padding@tue.nl

ABSTRACT

The kinetic theory of granular flow (KTGF) for dilute flows of smooth spheres is widely used in continuum modeling of gas-solid flows. In reality, granular particles are frictional and can achieve a state of dense packing, and these features must therefore be considered to improve the simulation of the hydrodynamics of dense gas-particle flows. In this study, the KTGF is extended to rough particles in dense systems, which includes rotation, sliding and sticking collisions using a simple moment method (Jenkins and Richman, 1985). The new KTGF has been incorporated into our in-house two-fluid model (TFM) code for the modeling of dense gas-solid fluidized beds. A critical comparison of a hard-sphere discrete particle model (DPM) and a TFM with the new KTGF in a pseudo-2D gas-fluidized bed is presented.

NOMENCLATURE

e	normal restitution coefficient
p	pressure, Pa
$\mathbf{v}$	velocity, m/s
$\mathbf{F}$	force, N
m	mass, kg
$\mathbf{T}$	torque, Nm
ρ	density, kg/m^3
Θ	granular temperature, m^2/s^2
β_0	tangential restitution coefficient
σ	particle diameter, m
γ	energy dissipation rate, kg/(m·s^3)
β_A	inter-phase momentum transfer coefficient
$\boldsymbol{\tau}$	stress tensor, Pa
ε	volume fraction
$\boldsymbol{\omega}$	rotational velocity, rad/s
κ	thermal conductivity, kg/(m·s)

INTRODUCTION

Gas-solid fluidized beds find a widespread application in processes involving combustion, separation, classification, and catalytic cracking (Davidson et al., 1985). Understanding the dynamics of fluidized beds is a key issue in improving efficiency, reliability and scale-up. Owning to enormous increase in computer power and algorithm development, fundamental modelling of multiphase reactors has become an effective tool.

In this work, an Euler-Euler approach (Kuipers et al., 1992; Gidaspow, 1994) has been used for the modelling. The Eulerian two-fluid model (TFM) can predict the flow behavior of granular systems with linear dimensions of the order of several meters. It has emerged as a very promising tool as a result of its compromise between computational cost and amount of detail provided. In TFM, both the gas phase and the solid phase are treated as fully interpenetrating continua which are described by separate governing balance equations of mass and momentum. The challenge of this model is to establish an accurate hydrodynamic and rheological description of the solid phase. State-of-the-art closures have been obtained from the kinetic theory of granular flow (KTGF), initiated by Jenkins & Savage (1983), Lun et al. (1984), Jenkins & Richman (1985), Lun et al. (1991), and Nieuwland (1995). The original KTGF models of Jenkins and Savage (1983), Lun et al. (1984), Jenkins and Richman (1985) and Gidaspow (1994) are derived for nearly elastic particles with translational motion only. Comparisons between TFM simulations based on this KTGF and more detailed discrete particle model (DPM) simulations of gas fluidization have been reported in the literature (Goldschmidt et al., 2004; Wang et al. 2013; Bokkers et al., 2004) and show good agreement for sufficiently smooth particles.

In reality, however, most granular materials are frictional. The roughness of the granular materials has been shown to have a significant effect on stresses at least in the quasi-static regime (Sun & Sundaresan, 2011). During a collision of rough particles, the particles can start to rotate due to surface friction. Thus, kinetic energies may be exchanged both translationally and rotationally. Attempts to quantify the friction effect have been somewhat limited in the past. In this work, the KTGF is extended to rough spheres, including particle friction and rotation. The rheological properties are explicitly described in terms of friction effects. This model has been incorporated into our in-house Euler-Euler code. Simulations of gas-solid fluidized bed are carried out. DPM is used as a research-tool to validate the new model.

NUMERICAL MODELS

Two fluid model

The two fluid model describes both gas phase and solid phase as fully interpenetrating continua. The continuity equations for gas and solid phases are given in equation 2.1 and 2.2. The momentum equations are given by 2.3 and 2.4.

$$\frac{\partial(\varepsilon_g \rho_g)}{\partial t} + \nabla \cdot (\varepsilon_g \rho_g \mathbf{v}_g) = 0 \qquad (1)$$

$$\frac{\partial(\varepsilon_s\rho_s)}{\partial t}+\nabla\cdot(\varepsilon_s\rho_s\mathbf{v}_s)=0 \tag{2}$$

$$\frac{\partial(\varepsilon_g\rho_g\mathbf{v}_g)}{\partial t}+\nabla\cdot(\varepsilon_g\rho_g\mathbf{v}_g\mathbf{v}_g)= -\nabla\cdot(P_g\mathbf{I}+\varepsilon_g\boldsymbol{\tau}_g)+\varepsilon_g\rho_g\mathbf{g}-\beta_A(\mathbf{v}_g-\mathbf{v}_s) \tag{3}$$

$$\frac{\partial(\varepsilon_s\rho_s\mathbf{v}_s)}{\partial t}+\nabla\cdot(\varepsilon_s\rho_s\mathbf{v}_s\mathbf{v}_s)= -\nabla\cdot(P_s\mathbf{I}+\varepsilon_s\boldsymbol{\tau}_s)+\varepsilon_s\rho_s\mathbf{g}+\beta_A(\mathbf{v}_g-\mathbf{v}_s)-\varepsilon_s\nabla P_g \tag{4}$$

The gas and solid phases are coupled through the interphase momentum transfer coefficient β_A. To describe the solid phase, KTGF with friction is used. In this work, particle surface friction and rotation are considered explicitly. In order to describe the solid phase rheology thoroughly, an extra energy balance equation for the rotational granular temperature was derived.

$$\frac{3}{2}\left[\frac{\partial(\varepsilon_s\rho_s\Theta_t)}{\partial t}+\nabla\cdot(\varepsilon_s\rho_s\mathbf{v}_s\Theta_t)\right]= -\nabla\mathbf{v}_s:(P_s\mathbf{I}+\varepsilon_s\boldsymbol{\tau}_s)+\varepsilon_s\nabla\cdot(\kappa_t\nabla\Theta_t)-\gamma_t-3\beta_A\Theta_t \tag{5}$$

$$\frac{3}{2}\left[\frac{\partial(\varepsilon_s\rho_s\Theta_r)}{\partial t}+\nabla\cdot(\varepsilon_s\rho_s\mathbf{v}_s\Theta_r)\right]= +\varepsilon_s\nabla\cdot(\kappa_{r1}\nabla\Theta_r+\kappa_{r2}\nabla\Theta_t)-\gamma_r \tag{6}$$

The definitions of the translational and rotational granular temperatures are $\Theta_t\equiv\langle C^2\rangle/3$, $\Theta_r\equiv I\langle\Omega^2\rangle/3m$, where I is particle's moment of inertia, C is the fluctuating translational velocity and Ω is the fluctuating angular velocity.

solid pressure: $\mathrm{P}_s=\varepsilon_s\rho_s\Theta_t\left(1+2(1+e)\varepsilon_s g_0\right)$

Bulk viscosity: $\lambda_s=(4/3)\varepsilon_s\rho_s\sigma g_0(1+e)\sqrt{\Theta_t/\pi}$

Solid stress tensor:

$$\boldsymbol{\tau}_s=-\begin{Bmatrix}(\lambda_s-2\mu_{t_s}/3)(\nabla\cdot\mathbf{v}_s)\mathbf{I}+\\ \mu_{t_s}[\nabla\mathbf{v}_s+(\nabla\mathbf{v}_s)^T]+\mu_{r_s}[\nabla\mathbf{v}_s-(\nabla\mathbf{v}_s)^T]\end{Bmatrix}$$

Rotational energy dissipation rate:

$$\gamma_r=\Theta_t g_0\rho_s\varepsilon_s^2\begin{Bmatrix}-\frac{96}{\sigma}\sqrt{\frac{\Theta_t}{\pi}}\left(2.5\mathrm{A}_2-\lambda\mathrm{A}_1\right)\\ +120\nabla\cdot\mathbf{v}_s\left(2.5\mathrm{A}_4-\lambda\mathrm{A}_3\right)\end{Bmatrix}$$

Rotational shear viscosity:

$$\mu_{r_s}=-8(2\lambda+1)\sigma g_0\rho_s\varepsilon_s^2\mathrm{A}_1\sqrt{\frac{\Theta_t}{\pi}}$$

Translational energy dissipation rate:

$$\gamma_t=g_0\rho_s\Theta_t\varepsilon_s^2\begin{Bmatrix}-\frac{192}{\sigma}\sqrt{\frac{\Theta_t}{\pi}}\begin{bmatrix}\eta_1(1+\eta_1)\\ -(2\lambda+1)\mathrm{A}_1\\ +(\lambda+1)\mathrm{A}_2\end{bmatrix}\\ +12\nabla\cdot\mathbf{v}_s\begin{bmatrix}\eta_1(1+\eta_1)+\\ 5[(\lambda+1)\mathrm{A}_4\\ -(2\lambda+1)\mathrm{A}_3\end{bmatrix}\end{Bmatrix}$$

Translational shear viscosity: $\mu_{t_s}=\bar{\mu}(1+\mu_{t_{s,c}})+\frac{3}{5}\lambda_s$,

$$\mu_{t_{s,c}}=-1.6\rho_s\varepsilon_s^2 g_0\sigma\left(-3(2\lambda+1)\mathrm{A}_1+\eta_1\right)\sqrt{\frac{\Theta_t}{\pi}}$$

Rotational thermal conductivity:

$\kappa_{r1}=\bar{\kappa}_{r,1}=\rho\Theta_t\left(L_3/2L_1\right)$,

$\kappa_{r2}=\bar{\kappa}_{r,2}=\rho\Theta_t\left(L_2/2L_1\right)$

Translational thermal conductivity:

$$\kappa_t=\bar{\kappa}_t(1+\kappa_{t_{s,c}})+\frac{3}{2}\lambda_s,$$

$$\kappa_{t_{s,c}}=-\rho_s\varepsilon_s\sigma g_0\sqrt{\frac{\Theta_t}{\pi}}\left(2\eta_1-16(2\lambda+1)\mathrm{A}_1\right)$$

Table 1: Closure equations.

Here λ is the rotational to translational granular temperature ratio. The expressions for A_1, A_2, A_3, A_4, A_9, A_{11}, A_{12}, L_1, L_2, L_3 can be found in Appendix A.

Discrete particle model

In DPM, the gas phase is described in the same way as in TFM (equations 2.1 and 2.3). However the solid phase is treated more detailed. The motion of every particle in the DPM is computed with Newton's second law of motion,

$$m_p\frac{d\mathbf{v}_p}{dt}=\sum\mathbf{F}=\mathbf{F}_{external}+\mathbf{F}_{contact}$$
$$I\frac{d\boldsymbol{\omega}}{dt}=\mathbf{T} \tag{7-8}$$

where m_p, $\mathbf{v}_p$, $\mathbf{T}$ are particle mass, velocity, and torque acting on the particle. The sum of all external forces acting on a particle $\mathbf{F}_{external}$ is calculated using:

$$\mathbf{F}_{external}=m_p\mathbf{g}-V_p\nabla p_g+\frac{V_p\beta_A}{1-\varepsilon_g}\left(\mathbf{v}_g-\mathbf{v}_p\right) \tag{9}$$

where V_p is the volume of particle. We use a linear spring-dashpot contact force, where the friction coefficient μ is limiting the tangential contact force:

$$\mathbf{F}_{contact,n}=-k_n\delta_n\mathbf{n}_{ab}-\eta_n\mathbf{v}_{ab}$$
$$\mathbf{F}_{contact,t}=\begin{cases}-k_t\delta_t-\eta_t\mathbf{v}_{ab,t}, & \text{(sticking)}\\ -\mu\left|\mathbf{F}_{contact,n}\right|\mathbf{t}_{ab}, & \text{(sliding)}\end{cases} \tag{10-11}$$

Where k_n, $\mathbf{n}_{ab}$, δ_n, η_n, $\mathbf{v}_{ab}$, δ_t, η_t are respectively the spring stiffness in the normal direction, the normal unit

vector, the overlap and damping coefficient in the normal direction, relative velocity at the contact point, and the overlap and damping coefficient in the tangential direction. We do not include a rolling friction. We refer to Hoomans et al. (1996) for details on the DPM model.

MODEL VALIDATION

Simulation settings

The DPM and TFM models have been implemented in our in-house codes. Because DPM is a much more detailed model, we use it to validate the newly-built TFM model based on kinetic theory. In the simulation, a no-slip wall boundary condition for side walls is used for the gas phase. At the bottom inlet, a uniform gas velocity is specified, whereas at the top outlet, atmospheric pressure (101.325 Pa) is prescribed. For the solid phase, a partial slip boundary condition is used for the side walls. Currently we use a relation for the solids velocity gradient and an expression for the pseudo Fourier fluctuation energy flux at the wall as given by Sinclair and Jackson (1989). The simulation settings are chosen based on those for relatively rough glass spheres (Goldschmidt, 2004) in a small system, and are given in Table 2. We note that the partial-slip boundary conditions employed in the TFM simulations are relatively time-consuming, especially for a quasi-2D system with large surface-to-volume ratio. As a consequence, the DPM and TFM simulations currently have comparable runtimes of the order of a few days for a total simulation time of 25 s, but no optimization attempts have been made yet on the TFM code.

Parameters	Values
Particle type	glass beads
Particle density, kg/m^3	2526.0
Particle diameter (mm),	2.0
Initial bed height (m),	0.09
Domain size (m),	0.09 × 0.012 × 0.36
Grid number (x × y ×z)	15 × 2 × 60
p-p collisional parameters,	e_n=0.97, β_0=0.33, μ=0.1
p-w collisional parameters,	e_w=0.97, β_w=0.33, μ_w=0.1
Specularity coefficient,	0.01
Superficial gas velocity,	2.5 U_{mf} (m/s)
Simulation time	25 s
Flow solver time-step	10^{-4} s

Table 2: Properties of particles and simulation settings.

Results and discussion

In this paper, the classical granular temperature due to random motion of individual particles in small regions during a small period is used. The global granular temperatures in the domain are calculated by,

$$\Theta_{t,global} = \frac{1}{3}\sum_{i}^{N_{part}} (\bar{u}_{t,i} - \left\langle \bar{u}_{t,p} \right\rangle_k)^2$$

$$\Theta_{r,global} = \frac{1}{3}\frac{\sum_{i}^{N_{part}} I_i}{\sum_{i}^{N_{part}} m_i} \sum_{i}^{N_{part}} (\bar{u}_{r,i} - \left\langle \bar{u}_{r,p} \right\rangle_k)^2$$

where $\left\langle \bar{u}_{t,p} \right\rangle_k$, $\left\langle \bar{u}_{r,p} \right\rangle_k$ are mass-averaged translational and rotational velocities for particles in cell k. N_{part} is the number of particles. The bed expansion dynamics is characterized by the averaged particle height,

$$\left\langle h_p \right\rangle_{bed} = \frac{\sum_{k}^{N_{cell}} \varepsilon_{s,k} h_k}{\sum_{k}^{N_{cell}} \varepsilon_{s,k}}$$

where N_{cell} is the number of cells in the domain.

The instantaneous porosities at different time obtained by different models are shown in **Figure 1**. It can be seen from the figure that large bubbles and densely packed regions are formed as a result of more energy dissipated due to particle rotation. Slugging fluidization is observed for both models. Thus, both models agree quite well.

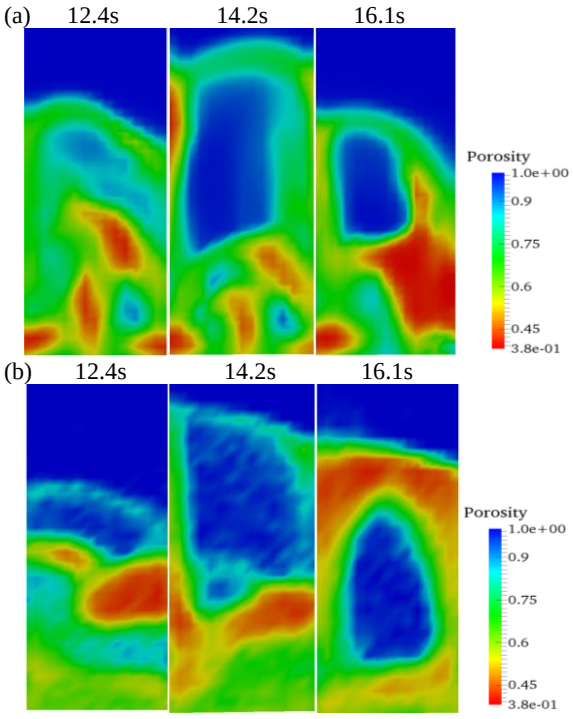

Figure 1: Instantaneous porosity in the fluidized bed. (a) TFM, (b) DPM.

Figure 2 shows the average particle height in the bed. The simulated results from TFM are very similar to those obtained from DPM, both for the average bed height and for the fluctuations in bed height.

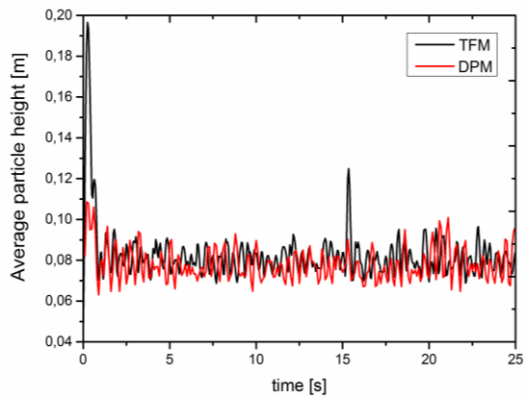

Figure 2: Comparison of simulated average particle height (see main text for details).

Figure 3 shows that good agreement between the TFM and DPM models can be obtained for the averaged translational and rotational granular temperature. The rotational granular temperature from TFM is somewhat higher than that from DPM. This can have two causes. First, in this dense situation the approximation of only binary collisions in KTGF starts to break down. Second, and probably more importantly, we assume a zero gradient of rotational granular temperature near the wall. This is not true in the real case. This indicates the need for development of accurate boundary conditions also for the rotational granular temperature.

(a)

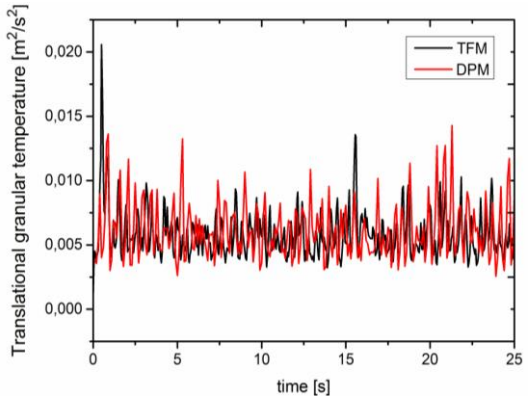

(b)

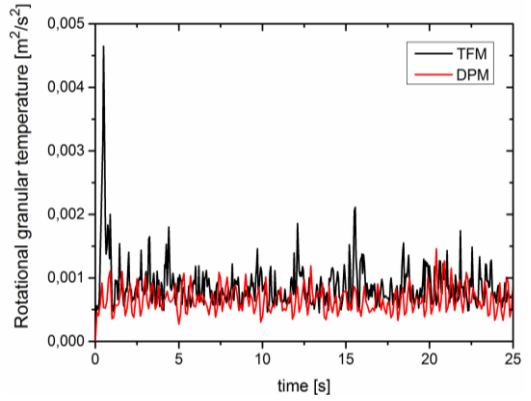

Figure 3: System-average granular temperatures in TFM and DPM simulations: (a) translational granular temperature; (b) rotational granular temperature.

For the solid circulation pattern, due to coalescence, the bubbles increase rapidly in size. As a consequence, a zone of increased bubble development, initially close to the wall near the gas inlet, is displaced towards the center of the bed with increasing height above the gas inlet. Particles appear to flow upwards in regions of more intense bubble activity and downwards in regions of lesser bubble activity, which results in the formation of a pronounced global solids circulation pattern. **Figure 4** shows that this kind of time-averaged macroscopic solids circulation pattern is qualitatively captured by the simulations and compares the solids circulation patterns of glass beads obtained from different simulation methods.

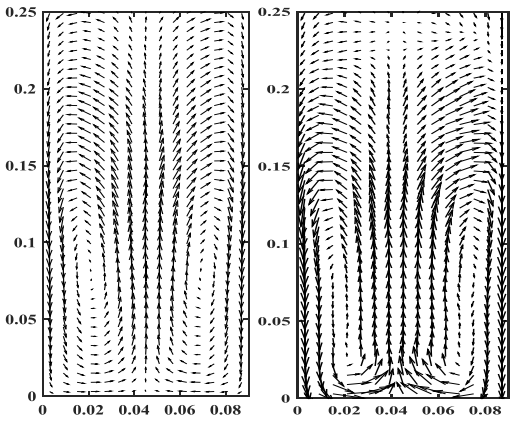

Figure 4: Comparison of time averaged solids circulation pattern (10-25 s), left-DPM modeling, right-TFM modeling.

Time-averaged porosity profiles from different models are shown in **Figure 5**. From the figure, it can be seen that small bubbles originate at the bottom of the bed, grow in size due to coalescence and move towards the central axis as a result of resistance at the center (Kunii and Levenspiel, 1991).

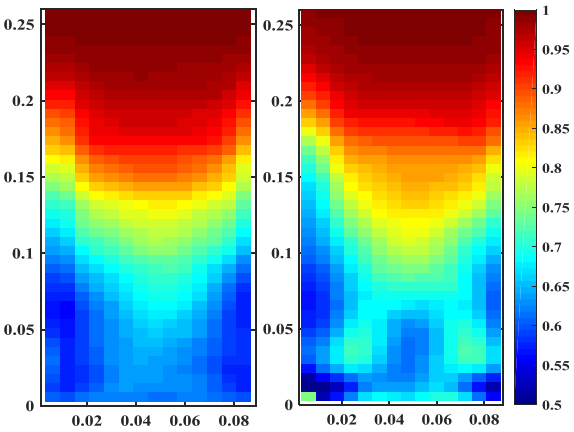

Figure 5: Comparison of time averaged porosity (10-25 s), left-DPM modeling, right-TFM modeling.

Figure 6 shows a comparison of time-averaged particle velocity components. For the lateral x-velocity component, particles show positive and negative velocities, in agreement with the pronounced global solids circulation pattern. The axial z-velocity is positive in the center regime and negative near the walls, which indicates that particles move upward in the center and flow down near the wall.

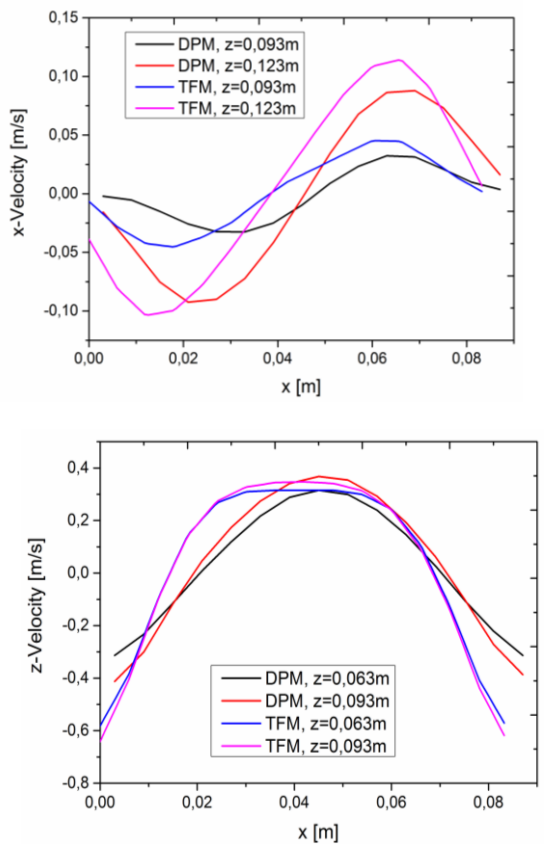

Figure 6: Comparison of time-averaged particle velocity components.

CONCLUSION & OUTLOOK

We developed a new KTGF for rough spheres. A detailed comparison between TFM using this new KTGF and a more detailed DPM model is performed, including translational and rotational granular temperatures, solids circulation pattern, axial and radial velocity profiles. For the first time, good agreement between two models is obtained for the rotational granular temperature. However, much work remains to be done. Despite the good qualitative agreement with DPM simulations, we find that it is essential to develop and implement correct boundary conditions for the rotational temperature and velocities of particles near the walls. .

REFERENCES

BOKKER, G.A., SINT ANNALAND, V.M., and KUIPERS, J.A.M., (2004). "Comparison of continuum models using the kinetic theory of granular flow with discrete particle models and experiments: extent of particle mixing induced by bubbles", 187-194.

DAVIDSON, J.F., CLIFF, R. and HARRISON, D. (eds), (1985), "Fluidization", 2nd ed. *Academic Press*, London, UK.

GIDASPOW, D., (1994), "Multiphase Flow and Fluidization: Continuum and Kinetic Theory Descriptions", *Academic Press Inc.*, Boston, USA.

GOLDSCHMIDT, M.J.V., BEETSTRA, R., and KUIPERS, J.A.M., (2004), "Hydrodynamic modelling of dense gas-fluidized beds: comparison and validation of 3D discrete particle and continuum models", *Powder Technology*, **142(1)**, 23-47.

HOOMANS, B.P.B., et al., (1996), "Discrete particle simulation of bubble and slug formation in a two-dimensional gas-fluidised bed: a hard-sphere approach." *Chemical Engineering Science* **51(1)**, 99-118.

JENKINS, J.T. and SAVAGE, S.B., (1983), "A theory for the rapid flow of identical, smooth, nearly elastic, spherical particles", *Journal of Fluid Mechanics*, **30**, 187-202.

JENKINS, J.T. and RICHMAN, M.W., (1985), "Grad's 13-moment system for a dense gas of inelastic spheres", *Archive for Rotational Mechanics and Analysis*, **87(4)**, 355-377.

JENKINS, J.T. and ZHANG, C., (2002), "Kinetic theory for identical, frictional, nearly elastic spheres", *Physics of Fluids*, **14**, 1228-1235.

KUNII, D. and LEVENSPIEL, O., (1991), "Fluidization Engineering", 2nd edition, Butterworth-Heinemann, Boston.

KUIPERS, J.A.M., VAN DUIN, K.J., VAN BECKUM, F.P.H. and VAN SWAAIJ, W.P.M., (1992), "A numerical model of gas-fluidized beds", *Chemical Engineering Science*, **47 (8)**, 1913-1924.

LUN, C.K.K., SAVAGE, S.B., JEFFREY, D.J. and CHEPURNIY, N., (1984), "Kinetic theories for granular flow: inelastic particles in curette flow and slightly inelastic particles in a general flow field", *Journal of Fluid Mechanics*, **140**, 223-256.

LUN, C.K.K., (1991), "Kinetic theory for granular flow of dense, slightly inelastic, slightly rough spheres", *Journal of Application Mechanics*, **233**, 539-559.

NIEUWLAND, J.J., (1995), "Hydrodynamic Modelling of Gas-Solid Two-Phase Flows", Ph.D. thesis, Twente University, Enschede, the Netherlands.

WANG, J., VAN DER HOEF, M.A. and KUIPERS, J.A.M., (2013), "Comparison of Two-Fluid and Discrete Particle Modeling of Dense Gas-Particle Flows in Gas-Fluidized Beds", *Chemie Ingenieur Technik*, **85(3)**, 290-298.

SINCLAIR, J.L. and JACKSON, R., (1989), "Gas-particle flow in a vertical pipe with particle-particle interactions", *AIChE Journal*, **l35**, 1473-1486.

SUN, J. and SUNDARESAN, S., (2011), "A constitutive model with microstructure evolution for flow of rate-independent granular materials", *Journal of Fluid Mechanics*, **682**, 590-616.

ZHAO, Y., LU, B. and ZHONG, Y., (2013), "Euler-Euler modeling of a gas-solid bubbling fluidized bed with kinetic theory of rough particles", *Chemical Engineering Science*, **104**, 767-779.

ACKNOWLEDGEMENT

The authors thank the European Research Council for its financial support, under its Advanced Investigator Grant scheme, Contract no. 247298 (Multi-scale Flows).

APPENDIX A

All the basic integrals which could be solved analytically using Mathematica, are listed as follows,

$$a_1 = (1+\lambda)\int_{\theta^*}^{\pi/2} \frac{\sin^2\theta_u \cos^2\theta_u}{(1+\lambda\cos^2\theta_u)^3} d\theta_u$$

$$a_2 = (1+\lambda)\int_{\theta 0}^{\theta^*} \frac{\sin^3\theta_u \cos\theta_u}{(1+\lambda\cos^2\theta_u)^3} d\theta_u$$

$$a_3 = (1+\lambda)\int_{\theta^*}^{\pi/2} \frac{\sin\theta_u \cos^3\theta_u}{(1+\lambda\cos^2\theta_u)^3} d\theta_u$$

$$a_4 = (1+\lambda)^{3/2}\int_{\theta^*}^{\pi/2} \frac{\sin^2\theta_u \cos^3\theta_u}{(1+\lambda\cos^2\theta_u)^{7/2}} d\theta_u$$

$$a_5 = (1+\lambda)^{3/2}\int_{0}^{\theta^*} \frac{\sin^3\theta_u \cos^2\theta_u}{(1+\lambda\cos^2\theta_u)^{7/2}} d\theta_u$$

$$a_6 = (1+\lambda)^{3/2}\int_{\theta^*}^{\pi/2} \frac{\cos^4\theta_u \sin\theta_u}{(\lambda\cos^2\theta_u+1)^{7/2}}$$

$$a_{10} = (1+\lambda)d\theta_u \int_{\theta^*}^{\pi/2} \frac{\sin^3\theta_u \cos^3\theta_u}{(1+\lambda\cos^2\theta_u)^4} d\theta_u$$

$$a_{14} = (1+\lambda)\int_{0}^{\theta^*} \frac{\sin^5\theta_u \cos\theta_u}{(1+\lambda\cos^2\theta_u)^4} d\theta_u$$

$$a_{15} = \int_{\theta^*}^{\pi/2} \frac{\sin\theta_u \cos^3\theta_u}{(1+\lambda\cos^2\theta_u)^4} d\theta_u$$

$$a_{16} = \int_{0}^{\theta^*} \frac{\sin^3\theta_u \cos\theta_u}{(1+\lambda\cos^2\theta_u)^4} d\theta_u$$

$$a_{17} = \int_{\theta^*}^{\pi/2} \frac{\sin^2\theta_u \cos^2\theta_u}{(1+\lambda\cos^2\theta_u)^4} d\theta_u$$

$$\mathrm{A}_1 = -(\mu\eta_1 a_1 + \eta_2 a_2)$$

$$\mathrm{A}_2 = (1+\lambda)\left[(\mu\eta_1)^2 a_3 + (\eta_2)^2 a_2\right]$$

$$\mathrm{A}_3 = -(\mu\eta_1 a_4 + \eta_2 a_5)$$

$$\mathrm{A}_4 = (1+\lambda)\left[(\mu\eta_1)^2 a_6 + (\eta_2)^2 a_5\right]$$

$$\mathrm{A}_9 = -(\mu\eta_1 a_{17} + \eta_2 a_{16})$$

$$\mathrm{A}_{11} = (\mu\eta_1)^2 a_{10} + (\eta_2)^2 a_{14}$$

$$\mathrm{A}_{12} = (\mu\eta_1)^2 a_{15} + (\eta_2)^2 a_{16}$$

$$L_1 = \frac{-32\varepsilon_s g_0}{25\sigma}\sqrt{\frac{\Theta_t}{\pi}}\begin{bmatrix} 50\,\mathrm{A}_2/\lambda - 10\,\mathrm{A}_1 - 10\,\mathrm{A}_{11}/3 \\ -50(\lambda+1)(\lambda+2)\,\mathrm{A}_{12}/(3\lambda) \\ +10(3\lambda+4)\,\mathrm{A}_9/3 \end{bmatrix}$$

$$L_2 = g_0\varepsilon_s\Theta_t\left[\frac{56\eta_1\lambda(\lambda+2)}{5(\lambda+1)} - 60(1+4\eta_1)(2\mathrm{A}_3\lambda - 5\mathrm{A}_4)\right]$$

$$L_3 = (1+\frac{12}{5}g_0\varepsilon_s)\lambda\Theta_t\left[-\frac{8\eta_1(2+\lambda)}{3(1+\lambda)} + 50(1+\eta_1)\mathrm{A}_3\right]$$

Note that for solid spheres we have: $\lambda = 2.5\Theta_r/\Theta_t$, $\eta_1 = -(1+e)/2$, $\eta_2 = -(1+\beta_0)/7$.